Structural Engineering and Mechanics, *Vol. 75, No. 1 (2020) 19-32*
DOI: https://doi.org/10.12989/sem.2020.75.1.019

Fatigue analysis of partly damaged RC slabs repaired with overlaid UHPFRC

Pengru Deng*[1], Ko Kakuma[2a], Hiroshi Mitamura[3b] and Takashi Matsumoto[1c]

[1]Faculty of Engineering, Hokkaido University, Sapporo, 060-8628, Japan
[2]Civil Engineering Research Institute for Cold Region, Sapporo, 062-8602, Japan
[3]The Calamity Science Institute, Sunbridge Co. Ltd, Sapporo, 007-0870, Japan

(Received September 9, 2019, Revised November 17, 2019, Accepted February 6, 2020)

Abstract. Due to repetitive traffic loadings and environmental attacks, reinforced concrete (RC) bridge deck slabs are suffering from severe degradation, which makes structural repairing an urgency. In this study, the fatigue performance of an RC bridge deck repairing technique using ultra-high performance fiber reinforcement concrete (UHPFRC) overlay is assessed experimentally with a wheel-type loading set-up as well as analytically based on finite element method (FEM) using a crack bridging degradation concept. In both approaches, an original RC slab is firstly preloaded to achieve a partly damaged RC slab which is then repaired with UHPFRC overlay and reloaded. The results indicate that the developed analytical method can predict the experimental fatigue behaviors including displacement evolutions and crack patterns reasonably well. In addition, as the shear stress in the concrete/UHPFRC interface stays relatively low over the calculations, this interface can be simply simulated as perfect. Moreover, superior to the experiments, the numerical method provides fatigue behaviors of not only the repaired but also the unrepaired RC slabs. Due to the high strengths and cracking resistance of UHPFRC, the repaired slab exhibited a decelerated deterioration rate and an extended fatigue life compared with the unrepaired slab. Therefore, the proposed repairing scheme can afford significant strengthen effects and act as a reference for future practices and engineering applications.

Keywords: UHPFRC; RC slab; bridging stress degradation concept; fatigue; moving wheel

1. Introduction

Over the past few decades, a brittle punching shear failure of reinforced concrete (RC) bridge deck slabs emerged as the most serious problem for a widely-employed slab-on-girder superstructure of highway bridges. It was reported that this unexpected failure mode is primarily attributed to the ignorance of slab shear capacity in old design specifications. In addition, except for the repetitive loadings from traffic, environmental actions, e.g. water, alkali-silica reaction (ASR) and freezing-thaw cycle (FTC), accelerated the structural deterioration and occurrence of failure (Maekawa *et al.* 2006, Matsui 1987, Mitamura *et al.* 2009, Ono *et al.* 2009, Maeshima *et al.* 2016). It was reported that the punching shear failure has been commonly observed around the world (Schläfli and Brühwiler 1998, Graddy *et al.* 2002, Perdikaris and Beim 1988), especially in Japan where the RC bridge deck slabs were designed with small thickness to achieve the maximum economic efficiency. Therefore, it is of great significance to develop effective repairing schemes for the deteriorated RC bridge decks to extend their service life and propose reliable analytical method for the repaired RC bridge decks to evaluate the effectiveness of the schemes.

In terms of the effective repairing scheme, to date, fatigue performance of RC slabs repaired with different cementitious materials have been investigated in many researches, where it was found that the fiber reinforced cementitious materials are the most effective, economic, and promising choices (Shah and Rangan 1971, Li 2002, Kanda *et al.* 2001). Owing to the existence of fibers, the material tensile and fatigue performances are remarkably improved. Several types of cementitious materials such as Fiber Reinforced Concrete (FRC) and Engineering Cementitious Composite (ECC) have been successfully employed in repairing RC slabs (Matsumoto *et al.* 2003, Suthiwarapirak and Matsumoto 2006). Recently, an Ultra-High Performance Fiber Reinforced Concrete (UHPFRC) was developed to satisfy the growing demand of repairing materials. This advanced composite material is composed of relatively large proportion of steel fibers, low water-binder ratio, and high micro silica content, which provide it with excellent workability and mechanical properties including self-compacting, high strength and modulus, strain-hardening behavior, and high fracture energy (Brühwiler and Denarié 2008, Richard and Cheyrezy 1995, Safdar *et al.* 2016). Under uniaxial compression or tension, the typical strength of UHPFRC reaches 150-200 MPa or 7-11 MPa, respectively (Bache 1987, Dugat *et al.* 1996, Rossi 2005, Habel *et al.* 2006). More importantly, UHPFRC exhibits extremely low permeability compared with the other cementitious materials and normal concrete (Brühwiler and

*Corresponding author, Assistant Professor, Ph.D.
E-mail: pengrudeng@eng.hokudai.ac.jp
[a] Ph.D.
E-mail: kakuma@ceri.go.jp
[b] Ph.D.
E-mail: mitamura@sunbridge.jp
[c] Professor, Ph.D.
E-mail: takashim@eng.hokudai.ac.jp

http://www.techno-press.com/journals/sem&subpage=7
ISSN: 1225-4568 (Print), 1598-6217 (Online)

Denarié 2013). Thereby, repairing the RC bridge decks with UHPFRC can additionally stop the penetration of the detrimental environment elements such as water and chloride ions to a great extent. Therefore, UHPFRC is the most suitable and promising repairing material for the RC bridge decks because the mechanical properties can improve structural load capacity and the low permeability characteristic can minimize the environmental causes of structural deterioration.

As for the reliable analytical methods, the fatigue life of RC slabs subjected moving wheel loads was predicted accurately on the basis of fracture mechanics with a crack bridging degradation concept (Deng and Matsumoto 2017, Deng and Matsumoto 2018, Deng and Matsumoto 2019). Moreover, based on the crack bridging degradation concept (Li and Matsumoto 1998, Matsumoto and Li 1999) and employing the FEM, fatigue analyses on both RC slabs and repaired RC slabs with ECC were conducted achieving a good coincidence between numerical and experimental results (Suthiwarapirak and Matsumoto 2006, Drar and Matsumoto 2016). The successful applications demonstrated the reliability of accessing fatigue performance of cement-based materials using the bridging degradation concept.

In this study, a repairing scheme with overlaid UHPFRC is applied on a partly damaged RC slab which is then tested under a moving wheel load experimental set-up. The partly damaged RC slab is obtained by preloading a healthy RC slab to a certain amount of cycles with the same set-up. In the meanwhile, fatigue behaviors of the repaired and unrepaired RC slabs subjected to the experimental stepwise loading sequence are analyzed by a numerical method developed by introducing the bridging stress degradation characteristics into three-dimensional FEM. In other words, the crack propagation due to bridging stress degradation is accounted as the dominant mechanism of structural degradation and inducing the fatigue failure. From analyses, the obtained results show a satisfactory agreement with the corresponding experimental results. Moreover, the effect of the overlay repair method is evaluated numerically for the purpose of the development of an appropriate repair design method. The numerical results demonstrate that the concrete/UHPFRC interface maintains a sound condition all through and the fatigue performance of the RC slab is remarkably improved owing to the high strengths of the overlaid UHPFRC. The remarkably extended fatigue life evidences the effectiveness of the repair method.

2. Experimental program

2.1 Materials and specimens

In this study, an original healthy RC slab specimen (S230) as shown in Fig. 1(a) is prepared as a reference to investigate the effects of UHPFRC overlay repair. The original RC slab which is designed following the Specification for Highway Bridges 2002 (JIS 2002) has a span of 2,350 mm, 3,300 mm and 2,650 mm along slab axis and transverse directions, respectively, and a thickness of 230 mm. The slab is reinforced with D19@125 mm center-to-center (c/c) and D16@125 mm c/c spacing along transverse and longitudinal directions, respectively, in the tension zone. In the compression zone, D19@250 mm c/c and D16@250 mm c/c spacing are equipped in longitudinal and transverse directions, respectively. All the reinforcing bars are made of SD345 steel (JIS 2004). Fig. 1(b) shows the detail information of the UHPFRC overlaid slab which is designated as RS190 where 190 stands for the slab depth in mm. Besides, in only analysis, an unrepaired RC slab (US190) which is same as the RS190 except for no UHPFRC repairing is investigated as well.

The slab was casted with normal concrete having the compression strength of 32.7 MPa and the Young's modulus of 21.7 GPa. All the SD345 reinforcing bars are with the yield strength of 345 MPa and the Young's modulus of 200 GPa. The concrete and reinforcement properties of the slab are given in Table 1. In terms of the UHPFRC, the material characteristics from tests conducted by the manufacturer are listed up in Table 2 for the design compression strength of 130 MPa. The ultra-high compression strength, i.e. 175 MPa, is obtained from compression tests, where the compression strength evolution along with the curing time was also measured as shown in Fig. 2(a). It is found that the UHPFRC achieved over 25 MPa and 100 MPa strengths at 2 hours and 1 day, respectively. This exhibited rapid hardening character makes it is very suitable for structural repairing as the traffic interruption can be minimized. After the first day, the strength increased gradually to 175 MPa at 28 days as displayed in Fig. 2(a). As for the material tensile behaviors, Fig. 2(b) shows its tensile stress vs. strain relation from uniaxial tensile tests in the laboratory. Superior to the normal concrete, UHPFRC exhibits some remarkable properties including a much higher tensile strength (11.5 MPa) and an apparent strain-hardening region resembling metals. At the maximum tensile strength, the average tensile strain reaches about 1300 μ attributed to

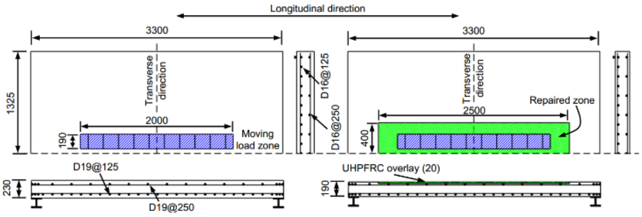

(a) Original slab (b) Repaired slab

Fig. 1 Slab geometry and reinforcement arrangement (Unit: mm)

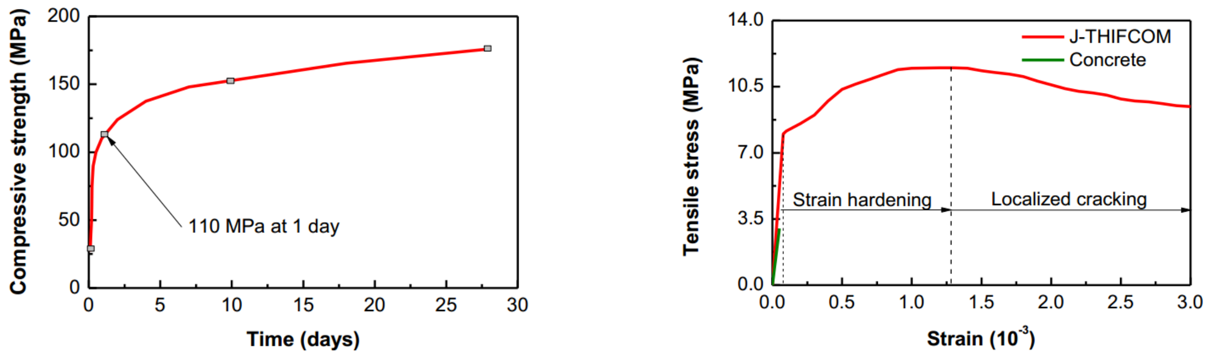

(a) Compression strength evolution (b) Tensile test

Fig. 2 Uniaxial test results of UHPFRC (Kosaka *et al*. 2015)

Table 1 RC Slab details

Parameters	Values	
Slab Dimensions	2650 mm×3300 mm	
Slab thickness (S230, S190)	230 mm→ 190 mm	
Transverse reinforcement	D19@125mm	Bottom
	D19@250mm	Top
Longitudinal reinforcement	D16@125mm	Bottom
	D16@250mm	Top
Concrete	E_c = 21.7 GPa	f_c' = 32.40 MPa
Steel	E_s= 200 GPa	f_y = 345 MPa

Table 2 Material characteristics of the UHPFRC (Kosaka *et al*. 2015)

Item	Test results	Remark
Compression	175 MPa	110 MPa at 1 day, over 130 MPa at 28 days
Uniaxial tensile	11.5 MPa	Crack strength 8.0 MPa
Young's modulus	35000 MPa	At 28 days
Bond	2.1 MPa	Base concrete crash
Shrinkage	0.0684 %	JSCE-K561-2010 at 28 days
Permeability	10-19 m^2	Torrent method

the widely-distributed small cracks. Except for the excellent mechanical properties, the torrent permeability test also confirmed its extremely low permeability (Kosaka *et al.* 2015). In addition, a slump flow test was carried out according to JIS R5201 (JIS 2015). The good flowability observed in the testing results (Fig. 3) demonstrated the good constructability of the material.

2.2 Moving wheel load test

A moving wheel load experimental set-up as shown in Fig. 4 was employed for conducting fatigue tests on the RC slabs in the Civil Engineering Research Institution (CERI) for Cold Region. The tested RC slabs are simply supported on the two edges along the bridge axis and elastically supported by I-girders along the other two edges. To prevent the uplifting of the four edges, uplift prevention devices were mounted on the four corners of the RC slabs. During the tests, the wheel load moves back-and-force on a

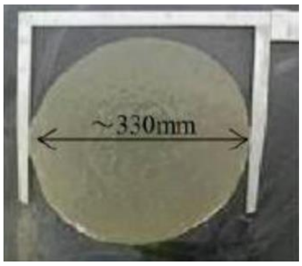

Fig. 3 Slump flow test result (Kosaka *et al*. 2015)

long iron plate of 12 mm thickness. To simulate the real wheel/bridge deck contact, the iron plate is supported by a series of isolated plates with a size 200 × 190 mm which is approximate to the contacting area size of a real wheel load. Correspondingly, a constantly distributed load was applied rather than a concentrated point load. As the purpose of this study is to investigate the repairing effectiveness of UHPFRC on the damaged RC slab, the original slab (S230) was pre-loaded with the moving wheel load machine under a stepwise loading sequence as shown in Fig. 5 until bending cracks appeared to obtain the partly damaged RC slab. And then, 20 mm layer of damaged concrete was removed from both the top and the bottom surfaces using a water jet method. As a result, the 230 mm thickness slab was turned into a 190 mm thickness slab. Thereafter, the RC slab was overlaid with a 20 mm thickness of UHPFRC in the middle portion through a patch repair with dimensions of 800 × 200 mm as displayed in Fig. 1(b). In this study, this overlaid slab is named as RS190 which was then loaded again with the moving wheel loading machine with a stepwise loading sequence as shown in Fig. 5. The stepwise loading sequence was employed to accelerate tests and investigate fatigue behavior of the RC slab under different loading levels. However, under this loading program, the obtained fatigue life is difficult to be used unless the numbers of loading cycles under different loading levels can be unified. In this study, this unification is conducted according to a slab S-N relation proposed by Matsui (Matsui 1987). Accordingly, the number of loading cycle (n_i) under any loading level (P_i) can be converted to the equivalent number of loading cycles (N_{eq}) under a given reference loading level (P) as follows:

$$N_{eq} = \sum \left(\frac{P_i}{P} \right)^m n_i \tag{1}$$

where *m* is the slope of S-N relation with a value of 12.76. This value was determined through fitting the fatigue life of RC slabs which have been subjected to the same moving wheel-type load with different loading levels (Matsui 1987). The employed reloading program is designed ensuring that the summation of the equivalent numbers of loading cycles under all the loading steps is equivalent to 2,000,000 for a 150 kN of reference load.

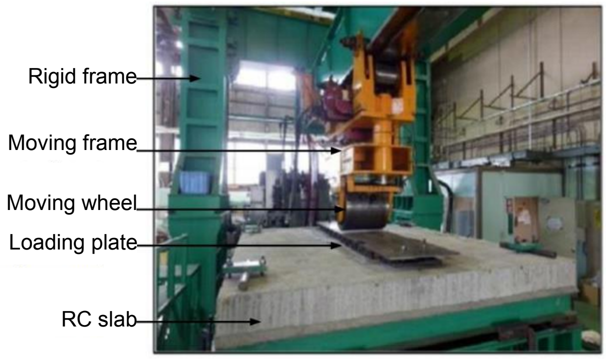

Fig. 4 Moving wheel load experimental set-up

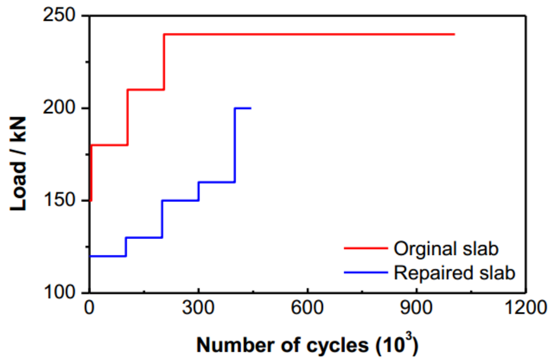

Fig. 5 Preloading and reloading programs

3. Fatigue analysis

3.1 Analytical models

The fatigue analyses of all the RC slabs are conducted based on the Finite Element Method (FEM) using an 8-node 3D element for all the structural members. A half of the slabs are modeled considering the symmetry of loading and boundary conditions. In the FE model of the original slab (S230) as shown in Fig. 6(a), the inner 6 layers between the tensile and compression reinforcing bars are modeled as RC element which means reinforcement is distributed in these layers, whereas two layers from the top and bottom surfaces are idealized as plain concrete element. The FE model of US190 is the same as that of S230 except for the removed one layer of concrete element from both the top and bottom surfaces. As for the repaired slab (RS190), the repaired zone in Fig. 1(b) is idealized as UHPFRC elements colored with green as shown in Fig. 6(b). To facilitate observation, RC element, concrete element, and UHPFRC element are shown with pink, yellow, and green colors, respectively, in the entire writing. The bond between concrete and UHPFRC is assumed to be perfect as no debonding at this interface was observed in experiments. The wheel load is applied by moving a distributed load on patch of the size of the wheel/slab contacting area along the longitudinal direction of the slab.

In the RC slab model, the concrete and UHPFRC are represented by smeared crack elements. Considering that both shear and flexural cracks could be the major causes inducing slab failure as observed from experiments and deteriorated RC slab under real traffic load, a multiple fixed crack model is employed to capture the crack formation and propagation characteristics of the cementitious materials. In this multiple fixed crack model, three perpendicular cracks are permitted to initiate at any integral point. Firstly, at any integral point, the crack named as the first set crack is assumed to initiate perpendicularly to the direction of the maximum principal strain once the tensile strain exceeds the cracking strain. Once the first set crack occurs, the co-ordinate is set up accordingly as shown in Fig. 7, where the N_1-axis is along the normal direction of the crack. And then, if the second tensile strain component exceeds the cracking strain, the second crack starts perpendicularly to the first crack. In the same way, the third crack forms perpendicularly to the existing two cracks. A Newton-Raphson iteration scheme is employed to obtain the solution of the effective stiffness matrix of the FE model containing nonlinear material constitutive relations (Ma *et al*. 1989). In order to speed up the calculation procedure, increments with more than 1 cycle may be used, normally five to 10 or 20 cycles. This depends on the loading level, fatigue crack growth rate, and the required accuracy. In this case, a linear interpolation of crack length in one increment has been used.

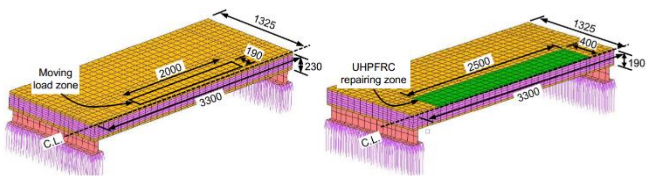

(a) Original healthy slab (b) Repaired slab with UHPFRC

Fig. 6 RC slab analytical models

(a) Initiation of a first crack (b) Three perpendicular cracks

Fig. 7 Crack formation

3.2 Material models

3.2.1 Concrete

In this study, the nonlinear behaviors of concrete under compression, tension, and shearing are considered. The uniaxial compressive stress-strain relation proposed by Maekawa (Maekawa *et al*. 2014) is employed as shown in Fig. 8(a), where the concrete stress increase nonlinearly to the peak stress with respect to an increasing strain and decrease linearly to zero at the limit compressive strain (ε_u). The concrete pre- and post-peak compression behaviors are given respectively as Eqs. (2)-(3).

$$\sigma = f_c{}' \frac{\varepsilon}{\varepsilon_m}\left(2-\frac{\varepsilon}{\varepsilon_m}\right),\quad 0 \ge \varepsilon \ge \varepsilon_m \tag{2}$$

$$\sigma = f_c{}' \frac{\varepsilon_u-\varepsilon}{\varepsilon_u-\varepsilon_m},\quad \varepsilon_m \ge \varepsilon \ge \varepsilon_u \tag{3}$$

where σ and ε are concrete stress and strain. ε_m is concrete strain corresponding to the compression strength of concrete, $f_c{}'$. The ultimate concrete compressive strain can be approximately related to ε_m as reported in (Maekawa *et al.* 2003).

$$\varepsilon_u = 3 \cdot \varepsilon_m \tag{4}$$

Under tension, the behavior of concrete is assumed linear elastic until the effective tensile strength before cracking (Eq. (5)).

$$\sigma = E_c \cdot \varepsilon,\quad \varepsilon_t \ge \varepsilon \ge 0 \tag{5}$$

where E_c is elastic modulus of concrete. ε_t is cracking strain of concrete which can be calculated as

$$\varepsilon_t = \frac{f_t}{E_c} \tag{6}$$

The effective tensile strength (f_t) is related to the concrete compression strength ($f_c{}'$) following the Japanese Specifications for concrete structures (JSCE 2007).

$$f_t = 0.23 \cdot f_c{}'^{2/3} \tag{7}$$

After cracking, due to the tension stiffening effect, concrete in RC members can still support part of the applied tension. This post-cracking tensile behavior is the fundamental difference between plain concrete and concrete in RC members. To model the average tensile behavior of concrete after cracking, the model (Eq. (8)) propsed by Shima (1986) is employed. The model is verified to be applicable to the targeted RC slab containing two-way reinforcement with ratios over 0.1~2.0% and independent to crack spacing, element size, and orientation of reinforcement in the element.

$$\sigma = f_t\left(\frac{\varepsilon_t}{\varepsilon}\right)^c,\quad \varepsilon \ge \varepsilon_t \tag{8}$$

$$\varepsilon = \frac{\delta_{cr}}{l} \tag{9}$$

where σ and ε are the average tensile stress and strain, respectively. c is stiffening parameter which equals 0.4 for

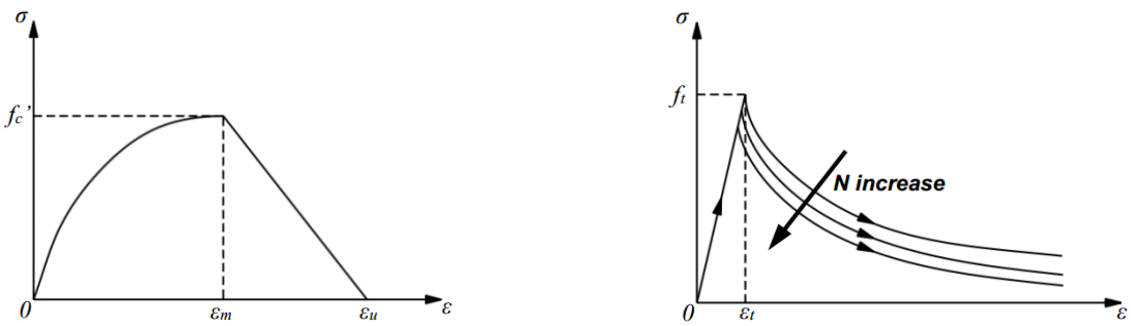

(a) Uniaxial compression stress-strain relation (b) Degrading tensile stress-strain relations under fatigue loads

Fig. 8 Stress-strain relations of concrete

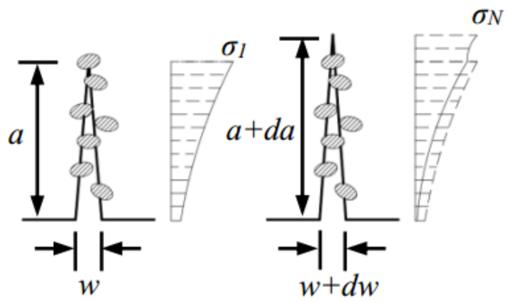

Fig. 9 Crack propagation after the 1st and Nth cycle due to bridging stress degradation

deformed bar. δ_{cr} is crack opening displacement and l is element size. As the model was derived using experimental results, the rebar/concrete interface bond-slip effect and the related tensile stiffening effect are implicitly included.

In addition, since the multiple fixed crack concept is employed and the generation of a crack in concrete is determined by the maximum principal stress, the shear transfer along crack planes needs to be addressed for the existing cracks. The concrete shearing behavior is determined according to a simplified shear transfer model which relates the shear stress with shear strain directly based on the contact density theory (Maekawa *et al*. 2014).

Under repetitive loads, the bridging stress degradation characteristic of concrete as shown in Fig. 8(b) is accounted for as the dominant degradation mechanism. For an existing crack with length a and width w, the repeated crack opening and closing process leads to the reduction of crack bridging stress, which means the concrete cannot transfer the same level of bridging stress with the same crack opening as the previous loading cycle. As a result, the crack propagates with an additional length, da, and additional width, dw, as shown in Fig. 9. For the concrete under single cyclic tension, the bridging stress degradation can be simply expressed using the maximum tensile strain, and number of loading cycles (Zhang *et al*. 1999).

$$\frac{f_{tN}}{f_t} = 1 - \left(d_0 + k\varepsilon_{t\max} l\right)\log\left(N\right) \tag{10}$$

where l is cracked element size, d_0 is stress degradation factor, k is slope of the linear relation between the bridging degradation factor and maximum tensile strain, f_{tN} and f_t are bridging stress at the Nth and the first cycle, respectively. Zhang et al. analyzed a large number of experimental data to conclude that the degradation of crack bridging stress under cyclic load is controlled by the number of cycles and the maximum and minimum crack opening. This degradation can be fitted by a linear model as a function of the logarithm of the number of cycles as shown in Eq. 10.
The degradation factor can be approximately related to the maximum crack opening as reported by Zhang *et al*. (1999), where it is found that d_0=0.08 and k=4mm^{-1} when the crack opening <0.016mm and d_0=0.014 and k=0.12 mm^{-1} when the crack opening >0.016mm. For smeared crack elements, the bridge stress degradation occurs by multiple cracks. Thus, the factor of the first range is applicable.

3.2.2 Reinforcing bar

In the employed smeared model, the reinforcement of the RC slabs is distributed with the reinforcement ratio in all directions. The stress-strain relation of reinforcement is represented by a bilinear curve which consists of a linear elastic stage and a linear hardening elastoplastic stage for steel stress lower and higher than the effective yielding stress, respectively, as shown in Fig. 10 (Shima 1986). Due to the bond in the rebar/concrete interface, local stresses of reinforcement are not uniform but vary along the bar axis. Thus, the steel at the crack vicinity yields earlier than other volumes. The post-yield average bar behavior must be modified based on the properties of the bare bar to include the bonding effect. For smeared idealization, the average yield stress is modified following an equation derived from a parametric study of Salem and Maekawa (1999) as

$$f_{y0} = f_y - \frac{f_t}{2\rho} \tag{11}$$

where ρ is the reinforcement ratio. f_y is the yield strength. f_t is concrete tensile strength. As for the non-yielded deformed bar in RC elements, the stress-strain relation of the bare bar is employed. The bond degradation due to the repetitive load is not considered because there is no report of RC slab failure due to fatigue rupture of reinforcing bars.

Under repetitive loads, the hysteretic behavior of a rebar as shown in Fig. 10 is represented by the Giuffrè-Menegotto-Pinto model expresses as following (Menengotto 1973):

$$\sigma^* = H\varepsilon^* + \frac{\left(1-H\right)\varepsilon^*}{\left[1+\left(\varepsilon^*\right)^R\right]^{1/R}} \tag{12}$$

$$R = R_0 - \frac{a_1\xi_{\max}}{a_1 - \xi_{\max}} \tag{13}$$

where ε* and σ* are the normalized strain and stress, respectively. H is hardening ratio, i.e. the ratio between the modulus of the second asymptote to the Young's modulus, have the value equal to 0.003. R is a parameter that influences the shape of the transition curve and takes account of the Baushinger's effect (Menengotto 1973). To describe this effect accurately, the parameter is considered to vary as a function of the maximum excursion in plastic range ξ_{max} of the previous loading path. R_0 is the value of R between elastic hardening for the first and Nth cycle, having the value equal to 20. a_1 and a_2 are experimentally determined parameters for the change of R with repetitive loading history, equaling to 18.5 and 0.00015, respectively.

3.2.3 UHFPRC

As shown in Fig. 1, the UHPFRC is paved for a thickness of 20 mm from the upper surface which stays in the compression zone of the RC slab under moving wheel load. The compressive behavior of this material must be accurately captured. In this study, a tri-linear stress-strain relation reported in (AFGC 2013) is employed to model the

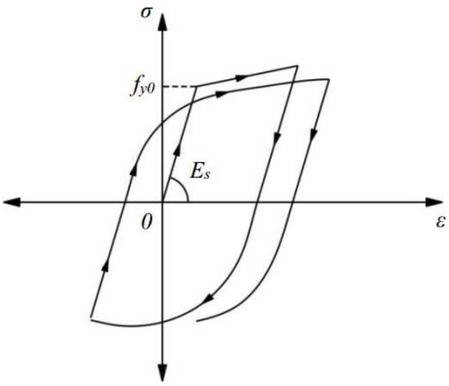

Fig. 10 Stress-strain relation of reinforcing bar

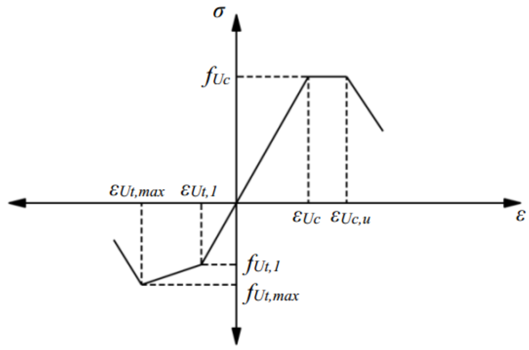

Fig. 11 Stress-strain relation of UHPFRC

uniaxial compression behaviors of UHPFRC as shown in Fig. 11. Firstly, the stress rises linearly to the compression strength (f_{Uc}) with the initial elastic modulus (E_{Uc}). Hereafter, the stress-strain relation reaches a plastic plateau until the average ultimate compression strain ($\varepsilon_{Uc,u}$). And then, the material stress drops dramatically with a high speed, showing a strong brittle characteristic. In this study, the experimentally obtained 28 days uniaxial compression strength (175 MPa) and initial elastic modulus (35 GPa) are assigned to f_{Uc} and E_{Uc}, respectively. The Poisson's ratio, υ_{Uc}, of UHPFRC is assumed as 0.22 which belongs to a range, 0.22~0.24, suggested in (Dugat *et al*. 1996).

3.3 Analytical procedure

Under the moving wheel loads, fatigue analyses of RC slabs with/without UHPFRC strengthening are conducted following the procedure illustrated in Fig. 12. In the experimental tests, the wheel load moves along the slab axis line. Thus, only a half of the slabs is modeled considering the symmetric boundary and loading conditions with respect to the slab axis.

At the first stage, firstly, a distributed load with a resultant force equaling to half of the experimental wheel load is applied on the four elements located at the center of the slab. The area of these elements is equivalent to that of distributed load. Repeating this unloading & loading process, the first loading cycle is completed following the routes indicated by the arrows as shown in Fig. 12(a). Secondly, the cracked elements due to the first loading cycle are recorded as shown in Fig. 12(a). Then, the constitutive model of the cracked elements is modified according to the bridging stress degradation concrete using the experienced stress history. Likewise, the slab fatigue behaviors after the second loading cycle can be obtained by applying one more loading cycle on the degraded slab. Finally, repeating the moving load following the preloading program shown in Fig. 5, one can obtain the degraded slab (S230) due to the preloading as in the experiments.

At the second stage, the slab model named as RS190 is obtained through removing one layer of elements from both top and bottom surface of S230 and then replacing the concrete element in the repairing zone (Fig. 12(d)) with the UHPFRC element initially. To facilitate investigating the effect of repairing, a slab model (US190) without repairing is prepared as well. With these two slab models, fatigue analyses are conducted under the loading program shown in Fig. 5 following the same procedure employed in the first stage. The analysis stops when the slabs lose the sectional force balance and the deflection increases rapidly. Finally, the reliability of the model and effectiveness of UHPFRC can be evaluated by comparing the experimental & numerical fatigue behaviors of RS190 and numerical fatigue behaviors of RS190 & US190, respectively.

4. Results and discussions

4.1 Propagation of cracked elements

According to the analytical procedure, the original RC slab (S230) is initially preloaded to obtain a degraded slab for repairing. Under the preloading program shown in Fig. 5,

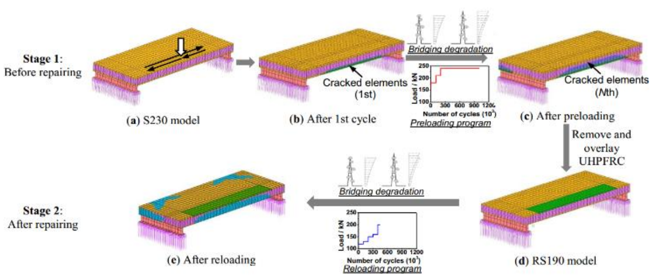

Fig. 12 Analytical procedure

the propagation of cracked elements is shown in Fig. 13(a) with different colors indicating the cracked elements after different number of loading cycles. The uncolored region represents uncracked zone.

Considering the slab symmetric characteristics along both the longitudinal and transverse directions, the oblique bottom view of a quarter of the slab model is shown in the figure. Incidentally, the view provides a clear view of the cracked element propagation along all the longitudinal, transverse, and vertical directions. It is found that the cracked elements expand from the region right below the moving load range to the joint corner point of the simple and elastic supports. This is caused by the force redistribution due to the degradation of the cracked element. Normally, the force redistribution of a structure tends to transfer in the direction with greater stiffness. As for the slab model, the joint point of the simple and elastic supports is the location with the maximum stiffness. In addition, as the wheel load moves along the slab axis in the longitudinal direction, it is found that the cracked elements are more fully distributed along this direction than the transverse direction. Due to the relatively high initial wheel load (150 kN), cracked elements are observed in the original RC slab after the first loading cycle as indicated by the blue area in Fig. 13(a). The cracked element volume increases to 48.3% of the whole slab volume after the loading cycle of 1,005,000 following the stepwise sequence preloading program shown in Fig. 5. Accordingly, the average propagation speed of cracked elements in the original slabs is 417.7 mm^3/cycle under the pre-loading program until the 1,005,000 loading cycle. Even though the cracked elements propagate up to 71% of the slab thickness along the vertical direction at the center of the original slab, the slab failure does not occur after the preloading program.

With the degraded slab S230, one can obtain analytical models of US190 and RS190, which are then loaded following the loading program shown in Fig. 5. The propagation of cracked elements in US190 and RS190 is shown respectively in Figs. 13(b)-(c), where the blue area represents the damage caused by the preloading in the original slab. The material properties of these elements are from the degraded slab S230. As 20 mm layer of elements are removed from the top and bottom surfaces of the degraded S230 to obtain US190 and RS190, the volume of cracked elements due to preloading is turned into 50.5% of the total volume of both slab models before reloading. It is found that, compared with that during the preloading, the cracked elements propagate into the inner layers at a much lower speed over the reloading program. This phenomenon is mainly attributed to the following three reasons: (1) since the slabs (US190 and RS190) are already cracked, the degradation rate is quite small according to Eq. (10); (2) for cracked element, the effect from reinforcement is superior to that from concrete, whereas no degradation of steel is assumed before yielding; and (3) considering that the slab thickness is reduced from the original 230 mm to 190 mm, the stepwise reloading program is designed with relative lower loading levels. As illustrated by Eq. (10), the bridging stress degradation is directly related to the maximum tensile strain. Thus, a small amount of degradation will be considered if the loading levels cannot generate tensile strain larger than the experience strain. Moreover, since the preloaded volume undergoes a large number of closing-opening processes, the slab without repair fails once the loading level increases to 200 kN at the 400,000 loading cycle. However, the repaired slab shows no failure even up to the 445,000 cycle, and the volume ratio of cracked elements is 60.6% which is even lower than the 61.2% observed in the unrepaired slab (US190) after failure.

Table 3 The percentage of cracked element volume

Slab	Test results 1st (%)	Test results Last loading (%)	Average degradation ratio (mm^3/cycle)	Remark
S230	6.7	48.3	417.7	Bending cracks
US190	50.5	61.2	810.0	Failure
RS190	50.5	60.6	188.3	No failure

The volume percentages of cracked elements in the three analyzed slabs are listed in Table 3 for some typical numbers of loading cycles. With the values appeared in the second and third columns, one can obtain the corresponding average propagation rates. It is indicated that the average propagation rate of the repaired slab is much smaller than that of the unrepaired and original slabs. The reason is that the overlaid UHPFRC reduces the slab deformations and delays the crack propagation, which in turn results in less reduction of bridging stress and less number of cracked elements in the analysis of slab US190.

4.2 Center displacement progression

For the original RC slab subjected to the preloading program, the numerically calculated and experimentally obtained center displacement evolutions with respect to the number of loading cycles is presented and compared as shown in Fig. 14(a). Due to the degradation of cracked elements and the resulting reduction of slab stiffness, the center displacement increases with the increasing number of loading cycles. From the figure, a close correspondence between the numerical and experimental results is observed throughout the specified cycles. However, the numerical result shows a steeper slope than that of the experimental result from 0 to 200,000 cycles. This is probably due to the significant reduction in the degradation ratio according to the bridging stress degradation concept (Eq. (10)) and the calculation increment scheme which is determined to achieve a balance between calculating efficiency and accuracy. Employing the same numerical model as in this study, the effect of calculation increment was investigated by Khan *et al*. (2018), where the steep slope faded away if a smaller calculation increment was adopted and the discrepancy between numerical and experimental decreased with the increment gets shorter. Therefore, the calculation increment should be selected carefully and the reduction of the concrete tensile capacity is a dominant degradation mechanism of RC slabs under fatigue loads.

Fig. 14(b) presents the experimental and numerical center displacement evolution curves of the repaired slab

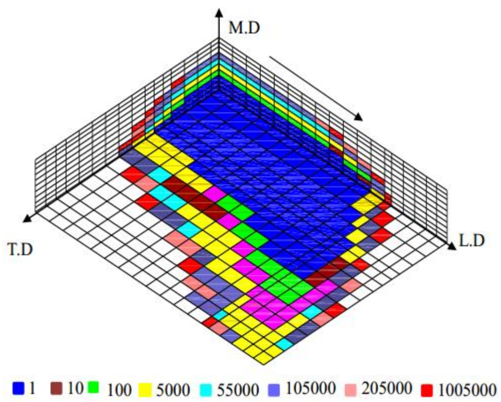

(a) Original slab

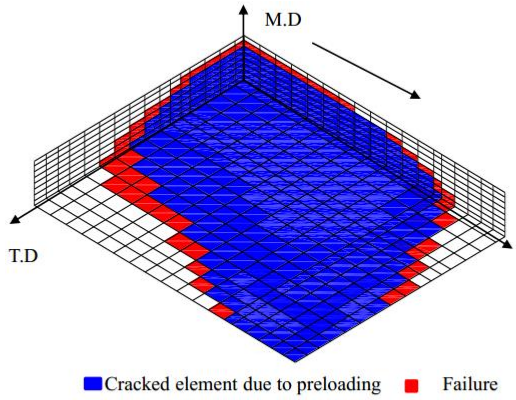

(b) Unrepaired slab

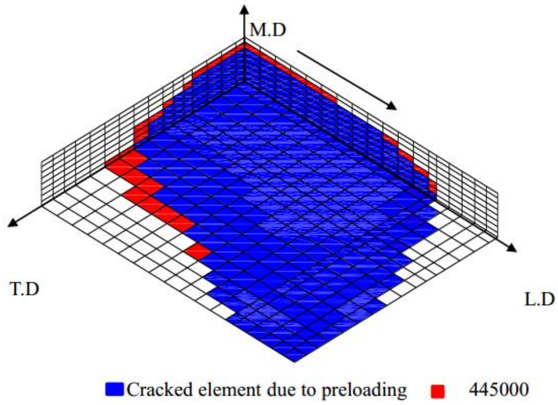

(c) Repaired slab

Note: M.D.: Moving Direction L.D.: Longitudinal Direction T.D.: Transverse Direction

Fig. 13 Propagation of cracked elements for different slabs

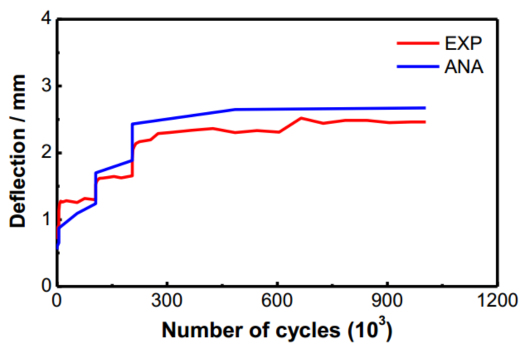

(a) Original slab

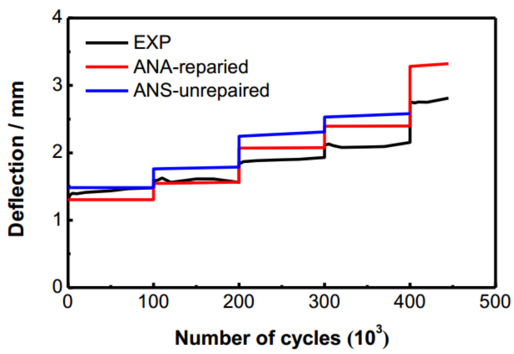

(b) Unrepaired and repaired slabs

Fig. 14 Center displacement evolutions

(RS190) as well as the numerical results of the damage unrepaired slab (US190). The repairing effect of the overlaid UHPFRC is clearly evidenced by the smaller center displacement of RS190 than that of US190. For the repaired slab under a certain loading level, due to the high strength and stiffness of UHPFRC, the center displacement exhibits only a marginal increase with the increasing number of cycles in both experiment and analyses. This can be understood similarly following the explanations for the decelerated cracked element propagation over the reloading program compared with that during the preloading program. Under the reduced loading levels during the reloading stage as shown in Fig. 5, the structural degradation which is due to the bending cracks created by the preloading should be very small according to the bridging stress degradation equation.

Due to fatigue loading, there is a repetitive crack opening and closing process which reduces the slab stiffness rapidly and ultimately significant increase in center displacement is observed. For repaired slab (RS190), the analytical center displacement evolution shows the accumulated difference of displacement at 200 kN at

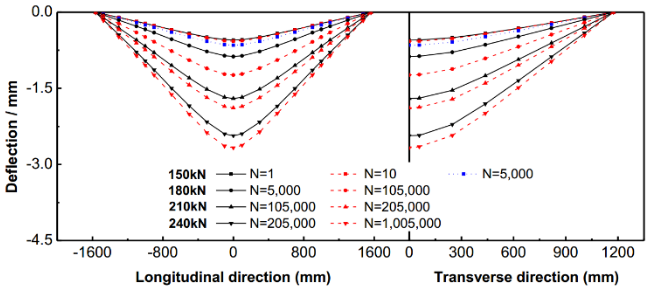

(a) Original slab under preloading

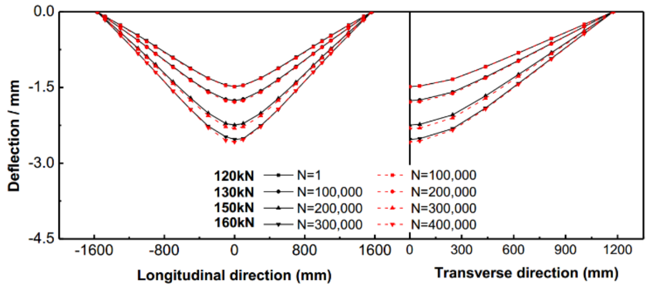

(b) Unrepaired slab under reloading

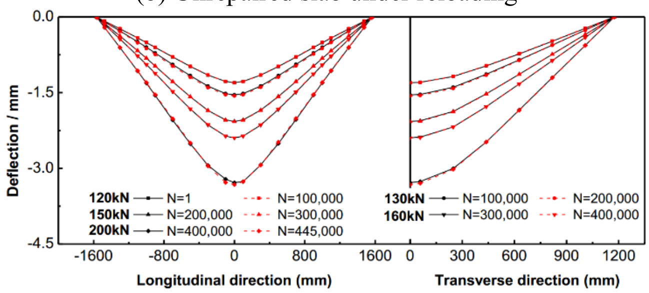

(c) Repaired slab under reloading

Fig. 15 Displacement distributions along L.D. and T.D. for different loading cycles

445,000 cycles when compared with the experimental observations. The experimental loading program was designed to achieve an equivalent 2,000,000 wheel runs under 150 kN loading level according to Eq. (1). The wheel load stops at 200 kN at 445,000 cycles. At this load, the overlaid slab did not fail in punching shear whereas the unrepaired slab (US190) failed at 400,000 cycles, which means the overlaid repairing technique with UHPFRC can provide sufficient fatigue capacity.

Figure 15 shows the displacement distributions along the longitudinal and transverse centerlines for the original RC slab (R230) under the preloading program and the unrepaired RC slab (US190) and repaired RC slab (RS190) under the reloading program. For each loading level in the stepwise loading process, these figures show only the displacement distributions at the starting and ending cycles to minimize mess and facilitate investigating the repeating effect of loading. From Figure 15(a), one can clearly observe the displacement increasing due to structural degradation. In addition, as the elements close to the slab center experience higher level of cracking strains, the extent of stiffness degradation increases from boundaries to the center. As a result, the displacement increasing becomes more localized in a certain region close to the slab center, especially for the two curved under the 240 kN of load where the displacement increasing shows an accelerating trend from the boundaries to the center of the slab. In terms of the displacement curves under the reloading program, due to the reduced loading level, displacement grows with a much slower speed than under the preloading program for both the repaired and unrepaired slabs. One can even barely observe the displacement increasing in the repaired RC slab. As for the unrepaired RC slab, even though the loading levels are reduced, the displacement still grows steadily with the increasing number of loading cycles, particularly around the slab center.

4.3 Maximum principal strain distribution

The comparison of maximum principal strain distributions on the bottom surface of the unrepaired and repaired slabs is shown in Fig. 16 for several loading levels. Only a quarter of the slabs are presented considering that the symmetric loading and boundary conditions of the slabs with respect to the longitudinal and transverse center lines when the wheel load moves onto the slab center point. To facilitate the comparison, the same strain range is selected to illustrate all the strain diagrams. Jointly investigating the two diagrams in one column, it is found that the unrepaired slab shows a slightly larger strain concentration than that of the overlaid slab. This is attributed to the extra stiffness and bending resistance provided by the overlaid UHPFRC

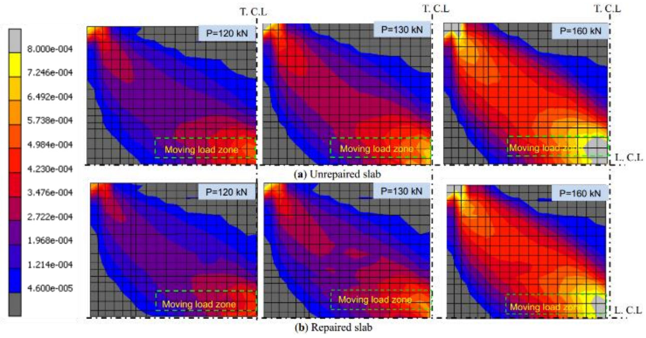

Fig. 16 Maximum principal strain distribution on the bottom surface

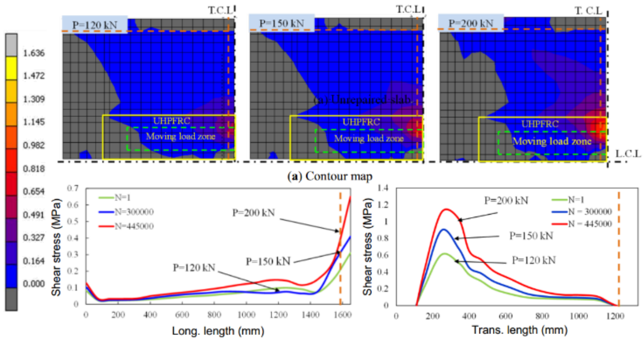

Fig. 17. Shear stress distributions at interfaces

compared with the normal concrete. Besides, owing to the good integrity of UHPFRC, the wheel load is more evenly distributed after transferred through the overlaid UHPFRC. Similar to the strain distribution on the bottom surface, theinner strain distribution of the unrepaired slab should be larger than the corresponding inner strain distribution of the repaired slab as well. According to the bridging stress degradation concept, more degradation occurs in the unrepaired slabs. As a result, the fatigue life of the slabs repaired with UHPFRC is considerably lengthened as shown in Fig. 14. Moreover, according to the stress distribution principal, the stress tends to distribute to the location with higher stiffness. As for the slab under the wheel load, the supporting corner is with the highest stiffness over the slab. Thus, the strain distributes in a diagonal direction from the loading point towards the supporting corner as shown in Fig. 16.

4.4 Shear stress distribution at interface

For structural repairing with cementitious materials, the interface condition determines its effectiveness and performance. In this study, as the UHPFRC is overlaid on the top surface of the slabs subjected to moving wheel load, the stress transferred in the concrete/UHPFRC interface is mainly the horizontal shear stress. Thus, the shear stress distribution on the bottom surface of the UHPFRC layer as shown in Fig. 17 is employed to evaluate the interface condition. The region encircled by the yellow rectangular is the area of concern. The shear stress contour maps reveal that the shear stress is concentrated near the loading point and is distributed mainly along the short, i.e. the transverse, direction. Figs. 17 show the shear stress distributions along the longitudinal and transverse center lines, respectively. It is found that, over the fatigue analysis, the shear stress increases with the increasing loading levels and cycles, and changes abruptly in the regions just adjacent to the loading point in both longitudinal and transverse directions. Specially, the shear stress in the transverse direction exhibits a more apparent increase compared with that in the longitudinal direction. In addition, as reported in Tayeh *et al*. (2013) that the interface shear strengthen varies from 8 to 12 MPa for different roughness in the concrete/UHPFRC interface, the shear stresses appeared in all conditions are much lower than the suggested strengths, which means the bond between substrate concrete and UHPFRC is not affected due to the moving load. Under such level of shear stress, the deterioration in the bond condition can be regarded as negligible and fatigue durability of the repaired slab is kept sound. Similar performances were observed after the experiments as well.

The shear strain distribution in transverse direction along with the cracking pattern and cutting section after the test are shown in Fig. 18. It is clearly observed from the analytical results that the shear strain is maximum in the diagonal direction from the loading point towards the slab hinge support. However, this localized shear deformation does not reach the concrete/UHPFRC interface. Thus, little effects are expected on bond durability. Moreover, a diagonal shear crack extending from the slab bottom surface towards to the loading point is observed in both the cutting section of tested slab and the analytical crack pattern. This oblique crack is generally named as punching shear crack. Even though the angle between the punching shear crack

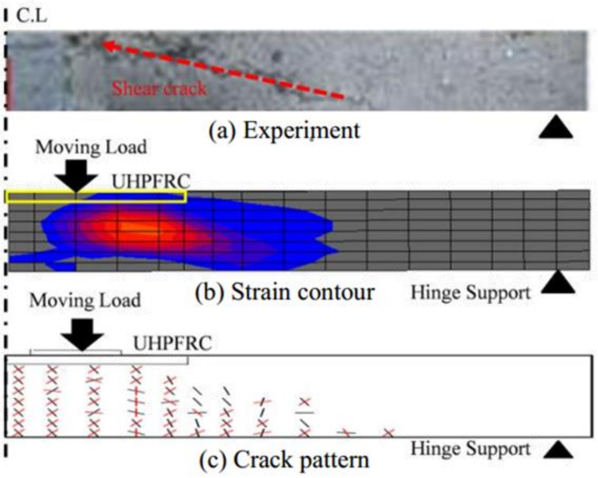

Fig. 18 Cut section after test and shear strain distribution in transverse direction along with the cracking pattern

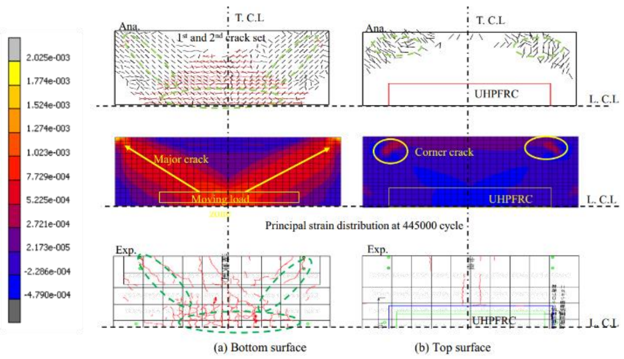

Fig. 19. Cracking pattern and maximum principal strain distribution for analytical and experimental repaired RC slab at 445,000

direction and the vertical direction is with similar value from both experiment and analysis, the angle is larger than that observed in tested RC slabs (i.e. 45°), which indicates that the overlaid UHPFRC shifts the failure mode from localized punching shear failure to the expected flexural failure. This shifting effect was observed in Steel Fiber Reinforced (SFRC) RC slab as well (Tanako *et al*. 2010, Abe *et al*. 2013). Fortunately, these cracks do not propagate to the UHPFRC layer and the interface due to the high cracking strength of UHPFRC.

4.5 Cracking pattern and maximum principal strain distribution

For the repaired RC slab at 445,000 loading cycle, the cracking patterns on both the bottom and top surfaces which are obtained from experiment and analyses are shown in Fig. 19. Generally, the analytical crack pattern shows a satisfactory agreement with that in experiment on both the bottom and top surfaces. Specifically, from the left column of diagrams for the bottom surface, it is found that the first main crack set appears from the slab center at the first moving load, thereafter, the main crack extends towards the supporting corners with the continuing movement of load. The maximum principal strain contour also indicates that the strain is localized beneath the loading point and distributed along the major crack direction. Similar to the diagonal cracks observed in the midspan cutting section as shown in Fig. 18, the diagonal cracks initiate and propagate all over the moving load zone in longitudinal direction as the wheel load moves onto the corresponding location. At the same time, flexural cracks perpendicular to the slab axis are formed as well, resulting in the grid cracks surrounding the moving load zone. Due to limitations of lab scale slabs, e.g. boundary conditions, the grid cracked zone is rather limited unlike the real extensive grid cracks. Thus, the grid cracks diminish away from the loading zone. In terms of the top surface of the repaired RC slab, Fig. 19 shows the comparison of the experimental and analytical cracking patterns together with the maximum principal strain contour on the surface. For the RC slab, an uplifting movement trend could be produced as the wheel load moves in the midspan. However, in analysis, hinge and elastic supports which can prevent both sagging and uplifting are set along the longitudinal and transverse edges, respectively. Due to this uplift preventing effect, tensile stresses in slab top surface may be generated in regions adjacent to the supports, especially around the corners. As a result, on the top surface of the repaired RC slab, a group of cracks initiate near each supporting corner and propagate along the longitudinal and transverse edges with the increasing loading levels and cycles. Correspondingly, the maximum principal strain contour map also illustrates that the strain is concentrated near corners on the top slab surface. In experiment, to prevent the uplift at slab corners, uplift prevention devices were set at the four corners. Obviously, the uplift prevention effect of the experimental BCs is not as strong as that in analyses. Hence, the generated tensile stresses in experiment did not induce cracks at the supporting corners. In terms of the regions near the repaired zone, the results indicated that very few cracks were formed during the experiment and no crack is formed in analysis. In addition, owing to the existence of the overlaid UHPFRC, no crack was observed in the rehabilitated part over the experiment and analysis, which demonstrates the improvement of fatigue performance with the proposed overlay repair method.

5. Conclusions

Aiming at extending the fatigue life of the severely deteriorated RC bridge decks, the effectiveness of a repairing technique, where an advanced cementitious composite, i.e. UHPFRC, was overlaid on a partly damaged RC slab, was assessed experimentally exploiting a wheel-type loading set-up and numerically based on a crack bridging degradation concept in FEM.

In the firstly stage, in both experiments and analyses, a partly damaged RC slab was achieved through preloading a healthy RC slab and then removing a certain thickness of concrete from top and bottom surfaces of the slab. The partly damaged RC slab was then repaired with a UHPFRC overlay obtaining a repaired RC slab which is further reloaded. Over the fatigue studies about the original RC slab and the repaired RC slab, the analytical results including midspan deflection, strain distributions, and crack patterns on both top and bottom surfaces exhibited an acceptable agreement with those from experiments, which verified the reliability of the proposed method. In addition, considering that the condition of the concrete/UHPFRC interface determines the collaboration between the new and old structural members, the interface shear stress was investigated. It was found that over the reloading program the experienced shear stress in the interface was much lower than the normal bond strength, which is because the concrete/UHPFRC interface bond strength is quite high and the localized shear stress along the diagonal direction did not reach the interface. In experiments, debonding was not observed as well. This good bonding condition demonstrated that the UHPFRC can be simply assumed as perfected bonded with concrete as conducted in this study.

In the second stage, superior to the experimental studies, fatigue analyses were performed on the partly damaged RC slabs with repairing as well as without repairing, where a straightforward image about the slab durability improvement owing to the repairing can be formed. The repaired slab exhibited a decelerated propagation of cracked elements, a reduction of midspan deflection, and a remarkable extension of fatigue life. In addition, the unrepaired RC slab reached the final failure under the reloading program, whereas fatigue failure did not occur in the repaired RC slab. All the improved fatigue behaviors evidenced the effectiveness of the proposed repairing scheme with overlaid UHPFRC. The superiority of this repairing technique may be even more obvious if the extremely low permeability is accounted for as the UHPFRC overlay can minimize the environmental attacks including water and chloride ions.

Conclusively, the developed numerical method with the crack bridging degradation concept can be exploited in assessing fatigue performance of RC slabs repaired with UHPFRC and the proposed repairing scheme with overlaid UHPFRC can be referenced in the future real engineering applications.

Acknowledgments

The authors would like to express their appreciation to the Prof. Shigeyuki Matsui of Osaka Institute of Technology, Mr. Tetsuya Okamura and Mr. Yasuo Kosaka for their valuable supports and discussions.

References

Abe, T., Suzuki, H., Kishi, Y. and Nomoto, K. (2013), “The effect of adhesive on the fatigue resistance of RC slabs strengthened by SFRC upper surface thickness increasing method”, *J. Struct. Eng.*, **59A**, 1084-1091. https://doi.org/10.11532/structcivil.59A.1084.

Association Française du Génie Civil (2013), “Bétons fibrés à ultra-hautes performances (Ultra high performance fibre-reinforced concretes)”, SETRA - Service d'études techniques des routes et autoroutes, AFGC.

Bache, H.H. (1987), *Introduction to Compact Reinforced Composite,* Nordic Concrete Federation

Brühwiler, E. and Denarié, E. (2008), “Rehabilitation of concrete structures using ultra-high performance fibre reinforced concrete”, *Proceedings of UHPC-2008: the 2nd International Symposium on Ultra-HighPerformance Concrete*, Kassel, Germany, 1-8. https://doi.org/10.2749/101686613X13627347100437.

Brühwiler, E. and Denarié, E. (2013), “Rehabilitation and strengthening of concrete structures using ultra-high performance fibre reinforced concrete”, *Struct. Eng. Int.*, **23**(4), 450-457. https://doi.org/10.2749/101686613X13627347100437.

Deng, P. and Matsumoto, T. (2017), “Weight function determinations for shear cracks in reinforced concrete beams based on finite element method”, *Eng. Fract. Mech.*, **177**, 61-78. https://doi.org/10.1016/j.engfracmech.2017.03.046.

Deng, P. and Matsumoto, T. (2018), “Determination of dominant degradation mechanisms of RC bridge deck slabs under cyclic moving loads”, *Int. J. Fatigue*, **112**, 328-340. https://doi.org/10.1016/j.ijfatigue.2018.03.033.

Deng, P. R. and Matsumoto. (2019), “Fracture mechanics based fatigue life prediction method for RC slabs in a punching shear failure mode”, *J. Struct. Eng.*, in press. https://doi.org/10.1061/(ASCE)ST.1943-541X.0002504.

Drar, A. A. M. and Matsumoto, T. (2016), “Fatigue analysis of RC slabs reinforced with plain bars based on the bridging stress degradation concept”, *J. Adv. Concr. Technol.*, **14**(1), 21-34. https://doi.org/10.3151/jact.14.21.

Dugat, J., Roux, N. and Bernier, G. (1996), “Mechanical properties of reactive powder concretes”, *Mater. Struct.*, **29**(4), 233-240. https://doi.org/10.1007/BF02485945.

Japan Road Association. (2002), *Steel bridge. Specification for Highway Bridges, Part III, Concrete Bridges*, Maruzen, Tokyo, Japan.

Japan Industrial Standard. (2004), “Steel bars for concrete reinforcement, JIS G-3112”, JISC, Japan.

Japan Industrial Standard. (2015), “Physical testing method of cement, JIS R-5201”, JISC, Japan

Japan Society of Civil Engineers. (2007), “Standard specifications for concrete structures-2007, design”, JISC, Tokyo, Japan

Graddy, J. C., Kim, J., Whitt, J. H., Burns, N. H. and Klingner, R. E. (2002), “Punching-shear behavior of bridge decks under fatigue loading”, *Strut. J.*, **99**(3), 257-266.

Habel, K., Denarié, E. and Brühwiler, E. (2006), “Structural response of elements combining ultrahigh-performance fiber-reinforced concretes and reinforced concrete”, *J. Struct. Eng.*, **32**(11), 1793-1800. https://doi.org/10.1061/(ASCE)0733-9445(2006)132:11(1793).

Khan, A. Q., Deng, P. and Matsumoto, T. (2018), “Development of an effective numerical model for fatigue analysis of RC bridge slabs”, *Proceeding of 10th Symposium on Decks of Highway Bridge*, Tokyo, Japan.

Li, V.C. (2002), “Large volume, high-performance applications of fibers in civil engineering”, *J. Appl. Polym.*, **83**(3), 660-686. https://doi.org/10.1002/app.2263.

Li, V.C. and Matsumoto, T. (1998), “Fatigue crack growth analysis of fiber reinforced concrete with effect of interfacial bond degradation”, *Cement Concrete Comp.*, **20**(5), 339-351. https://doi.org/10.1016/S0958-9465(98)00010-9.

Kosaka, Y., Imai, T., Mitamura, H. and Matsui, S. (2015), “Development of ultra-high performance fiber reinforced cement composite for rehabilitation of bridge deck”, *International Conference on the Regeneration and Conservation of Concrete Structures*, (RCCS), Nagasaki, Japan.

Kobayashi, K., Kano, Y. and Rokugo, K. (2014), “Example of composite deterioration of RC slab caused by ASR and frost attack in mountainous cold area and its verification”, *J. Jap. Soc. Cv. Eng.*, Ser. E2 (Matl. Concr. Struct.), **70**(3), 320-335.

Kanda, T., Saito, T., Sakata, N. and Hiraishi, M. (2001), “Fundamental properties of directed sprayed retrofit material utilizing fiber reinforced pseudo strain hardening cementitious composites", *Proceedings of Japan Concrete Institute*, **23**(1), 475-480.

Matsui, S. (1987), "Fatigue strength of RC-slabs of highway bridge by wheel running machine and influence of water on fatigue", *Proc., of Japan Concrete Institute*, **9**(2), 627-632.

Ma, S. Y. A. and May, I. M. (1986), "The newton-raphson method used in the non-linear analysis of concrete structures", *Comput. Struct.*, **24**(2), 177-185. https://doi.org/10.1016/0045-7949(86)90277-4.

Menengotto, M. (1973), "Method of analysis for cyclically loaded reinforced concrete plane frames including changes in geometry and nonelastic behavior of elements under combined normal force and bending", *IABSE Symposium on Resistance and Ultimate Deformability of Structures Acted on by Well-Defined Repeated Loads*, Lisbon, Portugal.

Maekawa, K., Gebreyouhannes, E., Mishima, T. and An, X. (2006), "Three-dimensional fatigue simulation of RC slabs under traveling wheel-type loads", *J. Adv. Concr. Technol.*, **4**(3), 445-457. https://doi.org/10.3151/jact.4.445.

Maeshima, T., Koda, Y., Iwaki, I., Naito, H., Kishira, R., Suzuki, Y. and Suzuki, M. (2016), "Influence of alkali silica reaction on fatigue resistance of RC bridge deck", *J. Jap. Soc. Cv. Eng.*, Ser. E2 (Matl. Concr. Struct.), **72**(2), 126-145.

Matsumoto, T. and Li, V. C. (1999), "Fatigue life analysis of fiber reinforced concrete with a fracture mechanics based model", *Cement Concrete Comp.*, **21**(4), 249-261. https://doi.org/10.1016/S0958-9465(99)00004-9.

Maeda, Y. and Matsui, S. (1984), "Punching shear load equation of reinforced concrete slabs", *Doboku Gakkai Ronbunshu*, **1984**(348), 133-141.

Maekawa, K., Okamura, H. and Pimanmas, A. (2014), "Non-linear mechanics of reinforced concrete", CRC Press, Florida, USA.

Matsumoto, T., Suthiwarapirak, P. and Kanda, T. (2003), "Mechanisms of multiple cracking and fracture of DFRCC under fatigue flexure", *J. Adv. Concr. Technol.*, **1**(3), 299-306. https://doi.org/10.3151/jact.1.299.

Mitamura, H., Satou, T., Honda, K. and Matsui, S. (2009), "Influence of frost damage on fatigue failure of RC deck slabs on road bridges", *J. Struct. Eng.*, **55A**, 1420-1431.

Ono, T., Mitamura, H., Hayashikawa, T. and Matsui, S. (2009), "Study on durability improvement of reinforced concrete slabs in snowy cold region", *J. Struct. Eng.*, **55A**, 1432-1441.

Perdikaris, P. C. and Beim, S. (1988), "RC bridge decks under pulsating and moving load", *J. Struct. Eng.*, **114**(3), 591-607. https://doi.org/10.1061/(ASCE)0733-9445(1988)114:3(591).

Rossi, P. (2005), "Development of new cement composite materials for construction", *Proceedings of the Institution of Mechanical Engineers, Part L: Journal of Materials: Design and Applications*, **219**(1), 67-74.

Richard, P. and Cheyrezy, M. (1995), "Composition of reactive powder concretes", *Cement. Concrete Res.*, **25**(7), 1501-1511. https://doi.org/10.1016/0008-8846(95)00144-2.

Shima, H. (1986), "Micro and macro models for bond behavior in reinforced concrete", Ph.D. Dissertation, The University of Tokyo.

Schläfli, M. and Brühwiler, E. (1998), "Fatigue of existing reinforced concrete bridge deck slabs", *Eng. Struct.*, **20**(11), 991-998. https://doi.org/10.1016/S0141-0296(97)00194-6.

Shah, S. P. and Rangan, B.V. (1971), "Fiber reinforced concrete properties", *J. Proc.*, **68**(2), 126-137.

Suthiwarapirak, P. and Matsumoto, T. (2006), "Fatigue analysis of RC slabs and repaired RC slabs based on crack bridging degradation concept", *J. Struct. Eng.*, **132**(6), 939-948. https://doi.org/10.1061/(ASCE)0733-9445(2006)132:6(939).

Salem, H. and Maekawa, K. (1999), "Spatially averaged tensile mechanics for cracked concrete and reinforcement under highly inelastic range", *Doboku Gakkai Ronbunshu*, **1999**(613), 277-293.

Safdar, M., Matsumoto, T. and Kakuma, K. (2016), "Flexural behavior of reinforced concrete beams repaired with ultra-high performance fiber reinforced concrete (UHPFRC)", *Compos. Struct.*, **157**, 448-460. https://doi.org/10.1016/j.compstruct.2016.09.010.

Tanako, M., Abe, T., Kida, T., Kodama, T. and Komori, A. (2010), "Fatigue resistance of RC slab overlaid with the SFRC determined by a fatigue test under running wheel load", *J. Struct. Eng.*, **56A**, 1259-1269.

Tayeh, B. A., Bakar, B. A., Johari, M. M. and Voo, Y. L. (2013), "Evaluation of bond strength between normal concrete substrate and ultra high performance fiber concrete as a repair material", *Procedia Eng.*, **54**, 554-563.

Zhang, J., Stang, H. and Li, V.C. (1999), "Fatigue life prediction of fiber reinforced concrete under flexural load", *Int. J. Fatigue*, **21**(10), 1033-1049. https://doi.org/10.1016/S0142-1123(99)00093-6.

PL